The QCAL tile calorimeter of KLOE

M. Adinolfi[a], F. Ambrosino[b], M. Antonelli[c], C. Bini[d], V. Bocci[d], F. Bossi[c],
P. Branchini[e,1], G. Cabibbo[d], R. Caloi[d], G. Carboni[a], M. Casarsa[f], G. Cataldi[g,2],
P. Ciambrone[c], S. Conetti[a,3], E. De Lucia[d], P. De Simone[c], S. Dell' Agnello[c],
A. Denig[c,2], A. Di Domenico[d], C. Di Donato[b], S. Di Falco[h], A. Doria[b],
A. Ferrari[e], G. Finocchiaro[c], C. Forti[c], A. Franceschi[c], P. Franzini[i,d], C. Gatti[c],
P. Gauzzi[d], S. Giovannella[c], E. Graziani[e,1], M. Incagli[h], C. Kuo[j], G. Lanfranchi[c],
M. Martemianov[c,4], W. Mei[c], R. Messi[a], S. Moccia[c], M. Moulson[c], S. Müller[j],
C.T. Murphy[k], F. Murtas[c], L. Pacciani[a], M. Palutan[e], E. Pasqualucci[d],
L. Passalacqua[c], A. Passeri[e,1], D. Picca[d], G. Pirozzi[b], L. Pontecorvo[d],
M. Primavera[g], E. Santovetti[a,*], G. Saracino[b], B. Sciascia[d], I. Sfiligoi[c],
T. Spadaro[d], E. Spiriti[e,1], P. Valente[c], B. Valeriani[j], G. Venanzoni[h,2], A. Ventura[g]

[a] Dipartimento di Fisica dell'Università e Sezione INFN, Roma II, Italy
[b] Dipartimento di Scienze Fisiche dell'Università e Sezione INFN, Napoli, Italy
[c] Laboratori Nazionali di Frascati dell'INFN, Frascati, Italy
[d] Dipartimento di Fisica dell'Università e Sezione INFN, Roma I, Italy
[e] Dipartimento di Fisica dell'Università e Sezione INFN, Roma III, Italy
[f] Dipartimento di Fisica dell'Università e Sezione INFN, Trieste, Italy
[g] Dipartimento di Fisica dell'Università e Sezione INFN, Lecce, Italy
[h] Dipartimento di Fisica dell'Università e Sezione INFN, Pisa, Italy
[i] Physics Department, Columbia University, New York, USA
[j] Institut für Experimentelle Kernphysik, Universität Karlsruhe, Germany
[k] Fermi National Accelerator Laboratory, Batavia, USA

Abstract

The quadrupole tile calorimeters of KLOE (QCAL) are two compact detectors placed close to the interaction point and surrounding the focusing quadrupoles. Their purpose is to increase the hermeticity of KLOE calorimetry. Each QCAL consists of a sampling structure of lead plates and scintillator tiles with wavelength shifter (WLS) fibers and mesh photomultiplier readout arranged in 16 azimuthal sectors. The arrangement of WLS fibers allows the

*Corresponding author. Dipartimento di Fisica, Universita di Roma "Tor Vergata", Via della Ricerca Scientifica 1, 00133 Roma, Italy. Tel.: +39-06-7259-4539; fax: +39-06-2025-364.

E-mail address: emanuele.santovetti@roma2.infn.it (E. Santovetti).

[1] Formerly Istituto Superiore di Sanità and Sezione INFN, ISS, Roma, Italy.
[2] Formerly Institut für Experimentelle Kernphysik, Universität Karlsruhe, Germany.
[3] Permanent address. University of Virginia, Charlottesville, USA.
[4] Permanent address. Institute of Theoretical and Experimental Physics, Moscow, Russia.

measurement of the longitudinal position of the showers from time of flight. In this paper we describe the QCAL design and assembly and present preliminary results obtained with both cosmic rays and photons from K_L decays. The time and energy calibration procedures are also discussed in detail. © 2002 Elsevier Science B.V. All rights reserved.

1. Introduction

The KLOE experiment [1] intends to do a precision study of CP violation in the K system. It is installed at the Frascati DAΦNE Φ-factory [2] where, at a luminosity of 3×10^{32} cm^{-2} s^{-1}, about 5×10^9 K_L–K_S pairs will be produced per year. This will allow the measurement of the direct CP violation parameter ε'/ε with a statistical error of about 10^{-4}, and systematic errors have to be kept less than this value. The parameter ε' is proportional $\langle \pi\pi | K_2 \rangle$ and is due to the direct CP violation in the decay amplitude $K_2 \rightarrow \pi\pi$. ε is a measure of CP violation in the mass term. An important issue is the control of systematic effects in background subtraction. The reaction $K_L \rightarrow \pi^0\pi^0\pi^0$ in which two photons are not detected can mimic the much rarer (~ 230 times) CP violating $K_L \rightarrow \pi^0\pi^0$ decay. In order to reduce such a background to a minimum, the hermeticity of the KLOE detector has to be maximized. In the original KLOE design, the major source of leakage

(about 80%) was due to photons absorbed by the two triplets of focusing quadrupoles, surrounding the beam pipe at about 50 cm from the interaction region (Fig. 1). Preliminary simulation studies [3] showed that without the QCAL calorimeters, 0.71% of the $K_L \rightarrow \pi^0\pi^0\pi^0$ events have two or more photons missing. With the QCAL this number is reduced to 0.14%, improving the potential rejection power by a factor of 5.

2. QCAL design

The main purpose of QCAL is tag photons in order to act as a $K_L \rightarrow \pi^0\pi^0\pi^0$ background veto. On the other hand, several mechanical constraints result in weight and thickness limitations. For this purpose we chose to maximize the photon detection efficiency in the range between 20 and 280 Mev (photons coming from $K_L \rightarrow \pi^0\pi^0\pi^0$ and $K_L \rightarrow \pi^0\pi^0$). The minimum time interval between consecutive bunch crossings at DAΦNE is 2.7 ns.
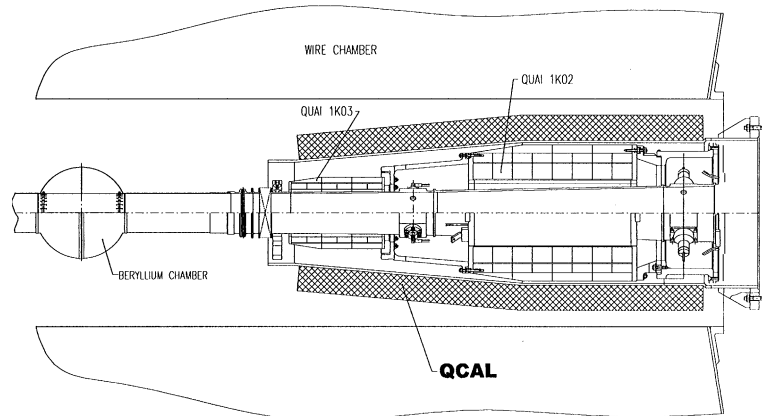

Fig. 1. One side of the interaction region. Two permanent quadrupoles are shown together with the surrounding calorimeter (QCAL).

In order to identify background contributions such as Bhabha scattering or machine background, a time resolution of ~ 1 ns (rms) is also needed, and this in turn requires a spatial measurement of the photon impact point. The optimal QCAL shape consists of a hollow cylinder connected to a truncated cone, fitting in the narrow space between the drift chamber inner tube and the beam focusing quadrupoles (Fig. 1).

2.1. Preliminary studies

One of the major problems faced in the QCAL design was the need to measure the impact point of the photon, since the inner face of the QCAL is not accessible. To solve this problem, we chose to divide the calorimeter radially into 16 sectors and to use optical fibers to collect the light inside each sector of the calorimeter. Sharing the same fibers between two sectors, by back-bending them from one sector to a non-adjacent other sector (Fig. 2), the longitudinal coordinate can be obtained from the time difference of the two collected signals.

Different types of fiber calorimeters were studied. Following the KLOE electromagnetic calorimeter (EMC) scheme [1], a sampling calorimeter solution with lead layers and scintillating fibers was first investigated. This solution provides a large light output and good time performance. Unfortunately, the large number of scintillating fibers in each sector (~ 1000) made the back bending of the fibers for sharing purposes impossible. We finally made the choice of a tile calorimeter with a wavelength shifting (WLS) fiber readout. This solution has a reasonably large light output and employs a small number of fibers, which is mandatory to allow the back bending.

Simulation studies have been performed to determine the thickness of the lead layers and of the scintillator tiles, in order to maximize the detection efficiency for a fixed total thickness of 5.2 cm. We chose 1 mm thick scintillator tiles and 2 mm thick lead planes. for each sector we put 15 scintillator layers and 16 lead layers, resulting in a depth of five radiation lengths for normally incident photons. Averaging over the incident angle, the sampling ratio is $\sim 4\%$, constant between 20 and 280 MeV, while the efficiency is shown in Fig. 3.

In this simulation, we cannot quote exactly the loss of efficiency resulting from WLS fiber light collection and, for this reason, it represents an upper limit of the true value. Given the low energy of the photons and the relatively small sampling
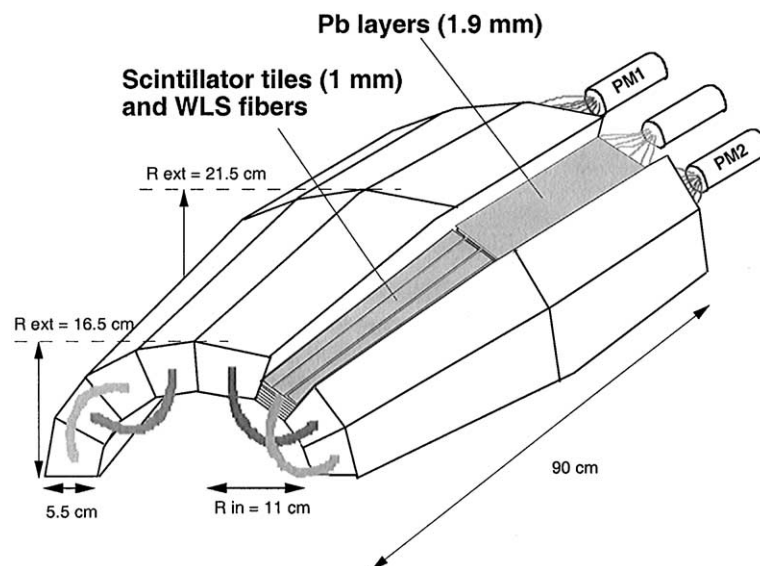

Fig. 2. Artist's view of the upper half of one QCAL calorimeter. Fibers connecting non-adjacent sectors are shown schematically.
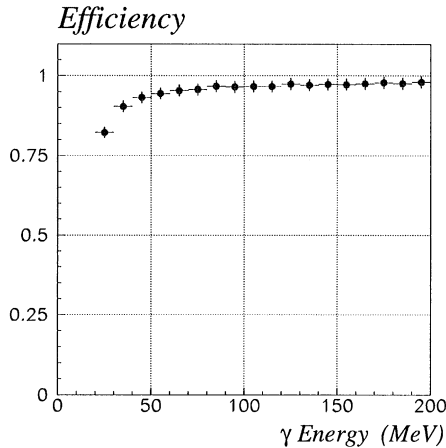
Fig. 3. Photon detection efficiency of the tile calorimeter (see text) versus photon energy from GEANT simulation.
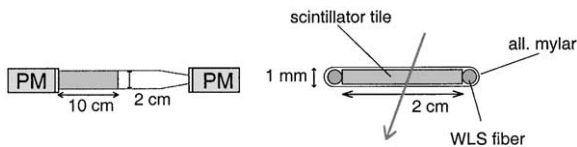

Fig. 4. Experimental setup for the light output measurement. On the left a top view is shown: The photomultiplier shown in the figure was used to measure the light from the fiber. On the opposite side, another photomultiplier directly coupled to the scintillator tile was used as the trigger. The tile and the two fibers are shown in cross-section on the right.

ratio, particular care has to be paid to enhance as much as possible the light output of the calorimeter. Several tests have been performed in order to evaluate the best scintillator and WLS fibers [8]. The light output of the tile–fiber coupling was the most crucial point and it was investigated for cosmic rays by means of the experimental setup schematically shown in Fig. 4.

A $(100 \times 20 \times 1)$ mm^3 scintillator tile was coupled to two WLS fibers along the two long thin faces. The fibers were simply air coupled to the tile, and the scintillator–fiber assembly was wrapped with white Tyvek paper. The light from the fiber was collected by a photomultiplier. In order to select cosmic rays, a trigger was provided by the triple coincidence between the fiber signal, a photomultiplier directly facing the scintillator on

the face opposite to the fibers output, and a third external scintillator counter. Table 1 summarizes the light yields for the different tested combinations of commercial scintillators and fibers. The best results were obtained with Bicron BC-408 coupled to Kuraray Y11-200, which were then chosen for the subsequent tests and for the final modules.

From GEANT simulation [7] both with photons and high energy muons, we found that a cosmic ray was equivalent to a 75 MeV photon in terms of visible energy inside the calorimeter. From this fact, using the measured photoelectron (p.e) yields with cosmic rays and the fact that the simulated sampling ratio is constant in the interesting energy range, one can infer a calorimeter response to photons of $\mathrm{d}n_{\mathrm{p.e.}}/\mathrm{d}E \simeq 0.5$ p.e./MeV.

Since the fibers are relatively long (~ 2 m), their attenuation length is important. In order to measure the fiber attenuation, we used the same setup of Fig. 4 with different fiber lengths. The results of these measurements are shown in Fig. 5. The points are well fitted by a double negative exponential with two attenuation lengths and relative weights quite similar for the three tested fibers ($R_1 \simeq 0.4$; $\lambda_1 \simeq 50$ cm; $R_2 \simeq 0.6$; $\lambda_2 \simeq 350$ cm).

The time resolution performance was studied using the setup of Fig. 6. To simulate with cosmic rays a signal equivalent to a 20 MeV photon (lower limit of the interesting energy range), four 1 mm thick scintillator tiles were superimposed and read by bundling the eight fibers together. The length of the eight fibers was chosen to be the one corresponding to the final QCAL modules ($\simeq 2$ m). Two photomultipliers[5] were used to collect the light from each side of the fibers, and their signals were fed to an ADC[6] and a TDC.[7]

Since the photomultiplier gain was set to $\simeq 2 \times 10^6$ and the output signal was amplified by a factor of 3, we can make the equivalence 1 MeV $\simeq 0.5$ p.e. $\simeq 0.85$ pC output from the photomultiplier. The results are summarized in Figs. 7 and 8. The average time resolution is $\sigma(t_z) =$

Table 1
Number of photoelectrons (p.e.) for the different WLS fibers (two lines) and scintillator (three columns) combinations. In parentheses the fraction of the scintillator light collected by the fibers is given

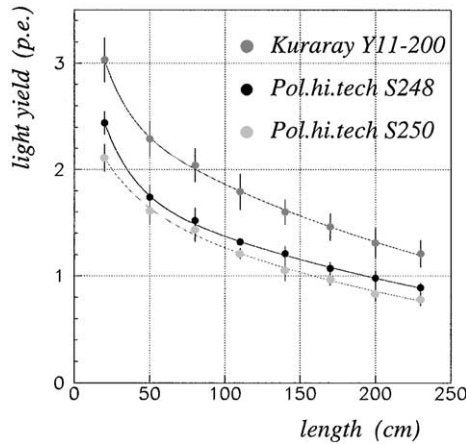| WLS fibers	Scintillator		
	Bicron BC408	Bicron BC404	Pol.Hi.Tech.
Kuraray Y11-200	3.4 (21.8%)	3.1 (18.2%)	2.1 (18.7%)
Pol.Hi.Tech. S248	2.8 (17.5%)	2.8 (16.6%)	1.8 (16.2%)

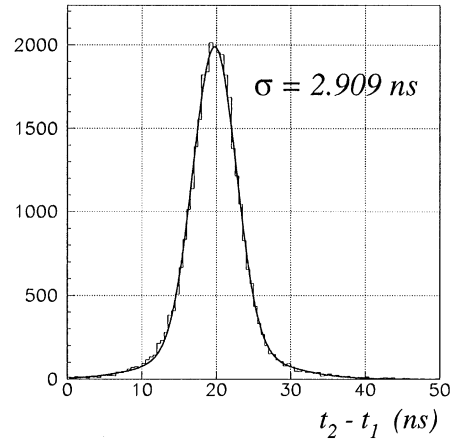Fig. 5. Number of photoelectrons as a function of the fiber length.

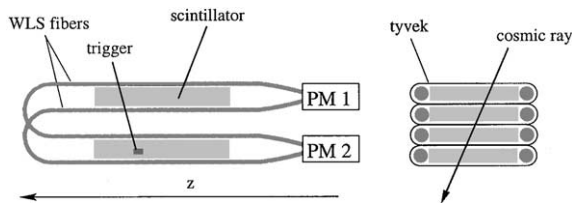Fig. 7. $t_2 - t_1$ distribution.

Fig. 6. Experimental setup used to measure the time resolution of a tile calorimeter.

$\frac{1}{2}\sigma(t_2 - t_1) \simeq 1.45$ ns, quite satisfactory for our needs. We also observed a clear correlation between the time resolution and the signal amplitude. As expected, the time resolution improves with increasing signal amplitude, the overall behavior being well described by the fit $\sigma(t_z) = 7/\sqrt{Q \text{ (pC)}}$ ns $= 205/\sqrt{E \text{ (GeV)}}$ ps.

3. Construction

The QCAL, consisting of a 50 cm long truncated conical part in the inner region closer to the interaction point and a 31 cm long cylindrical part in the outer region, is divided into 16 azimuthal sectors. The fibers exiting from the cylinder's end are brought onto photomultipliers (Figs. 1 and 2). The mechanical support consists of two 6 mm thick aluminum half shells placed around the inner quadrupoles, conical in the inner region and cylindrical in the outer one. Aluminum ribs 2 mm thick, screwed to the two shells, separate the 16 sectors. Each sector (Fig. 9) contains 16 absorber plates made of 2 mm thick lead, alternating with 15 scintillator layers 1 mm thick. The scintillator layers are divided into 3 equal tiles. In the cylindrical section the tiles have rectangular shape while in the conical one the shape is trapezoidal. In each layer, four 190 cm long
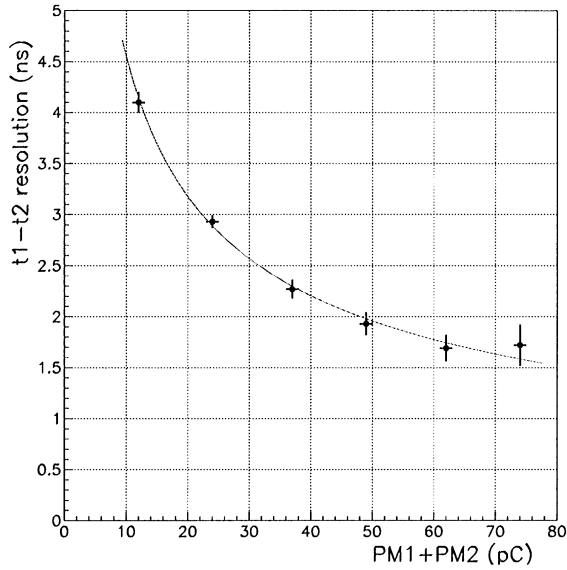
Fig. 8. Time resolution $\sigma(t_2 - t_1) = 2\sigma(t_z)$ as a function of the signal charge. The points are well fitted by the function $\sigma = 14/\sqrt{Q}\,(\text{pC})$ ns.

Fig. 10. The forward part of the QCAL calorimeter during the construction. The same fibers are used to collect the light of two non-adjacent sectors.
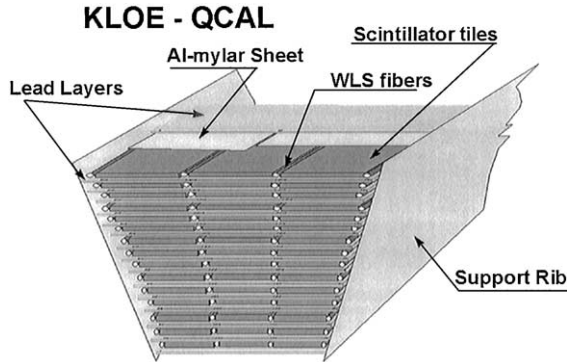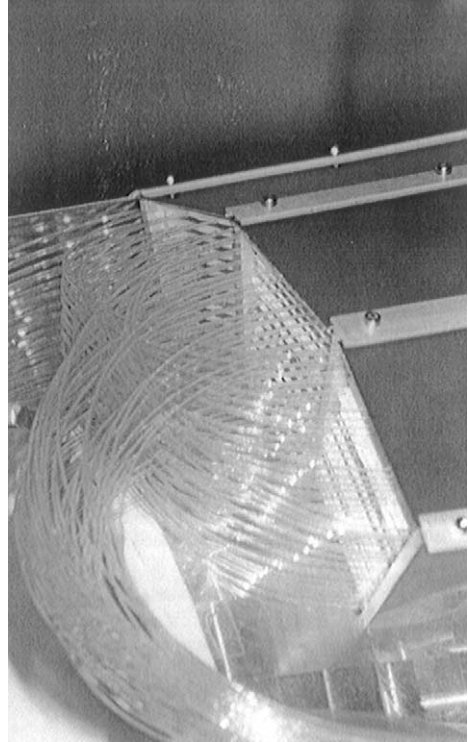

Fig. 9. A sector of the QCAL. Note the lead plates and the scintillator layers divided into 3 tiles. Four WLS fibers run along the tiles. The scintillator tiles and fibers are wrapped together in Tyvek paper to increase light collection.

WLS fibers run along the sides of the tiles. Several tests with different tile widths were performed in order to maximize the light output and the scintillator layer homogeneity, the four fiber solution resulting in the best compromise. Each layer of scintillator and fibers is wrapped in a Tyvek paper sheet to increase light collection. The

overall radial thickness is 5.2 cm (~ 5.5 radiation lengths).

Since both ends of each scintillator must be read out by the fibers to allow the measurement of z, a bundle is shared between two sectors (Figs. 2 and 10). From our simulation studies, a non-negligible fraction (about 30%) of the photons have showers extending into two adjacent sectors, while the number of events with showers extending over three adjacent sectors is only $\sim 4\%$. Therefore, in order avoid ambiguities, each sector is connected to the first non-adjacent sector (Fig. 2). This arrangement also allows a radius of curvature of the fibers much larger than 4 cm, without any stress on the fibers. The 60 WLS fibers of each sector are glued together, cut, polished and optically coupled to the photomultipliers. The signal arrival time is measured at both fiber ends and the longitudinal coordinate z is obtained from

the equation $z = L - v(t_2 - t_1)/2$, where L is $\frac{1}{2}$ of the total fiber length, v is the light velocity in the fiber, and t_1 and t_2 are the signal arrival times.

4. Readout and electronics

The photomultipliers have to operate in a longitudinal magnetic field of about 0.6 T. For this reason we adopted "mesh-dynode" photo-multipliers. They have a quantum efficiency of $\simeq 23\%$ and a gain of $\sim 2 \times 10^6$ without magnetic field. At $B = 0.6$ T a gain reduction of 60% is quoted [4]. To reduce noise, a ground cathode configuration is adopted and to increase reliability, the photomultiplier base is just a passive resistor divider, while HV decoupling capacitors and amplifiers are positioned in a separate and more accessible location. A special triaxial cable (~ 50 cm) is used to bring the signal, the high voltage and the reference ground from the photo-multiplier to the preamplifier board, one for each channel. We selected a current feedback pream-plifier[8] with a gain of three and a rise time of 2.5 ns. The output signal is sent to a special splitter board producing a shaped signal for the ADC and a discriminated one for the TDC [5].

5. Results

The QCAL calorimeters have been operational since the startup of the KLOE experiment (1999), acquiring first cosmic rays and then machine events. As expected, turning on the magnetic field causes a reduction of the photomultiplier gain of about 60%. In spite of the fact that the position of the photomultipliers is very close to the beam pipe and separated from the preamplifier board, the average ADC pedestal root mean square is equivalent to $\frac{1}{20}$ of the minimum ionizing particle (MIP) signal.

---

[8] Analog Devices AD8001.

5.1. Detection efficiency

As already mentioned, the fundamental task of the QCAL calorimeters is the photon detection efficiency in the energy range (20–280) MeV. A first measurement of the efficiency has been performed using cosmic rays, which deposit the same energy as a 75 MeV photon in QCAL. The drift chamber was used to track the cosmic ray inside the QCAL with a precision of $\simeq 3$ mm. Whenever the cosmic ray crossed one of the QCAL towers, we looked for a TDC signal from the photomultiplier directly coupled with this tower. The efficiency of a single tower, plotted in Fig. 11, has an average value of 98%. The efficiency for receiving both the signals of the two joined towers is 75%, and only for these events can we measure the z coordinate from TOF.

For events for which z can be determined, a study of the cosmic ray efficiency versus the impact point z coordinate and the ϕ radial angle has also been performed (Figs. 12 and 13). From the first plot we can check the right longitudinal position of the two calorimeters with respect to the rest of the apparatus. The small peak at large z is due to the Cherenkov photons produced in the photomulti-plier glass.

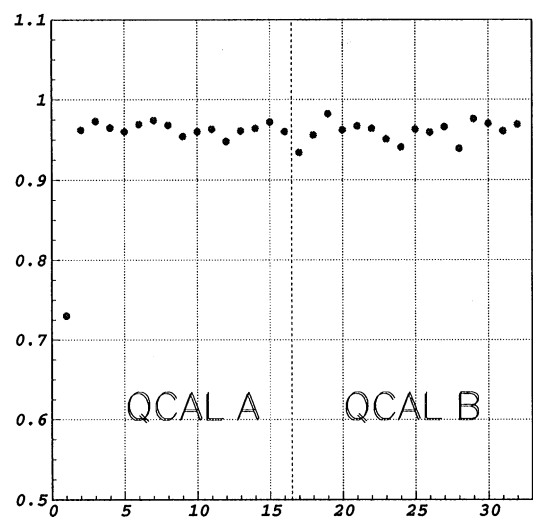In Fig. 13 the loss of efficiency arising from the support ribs (4 mm thick) between the towers is
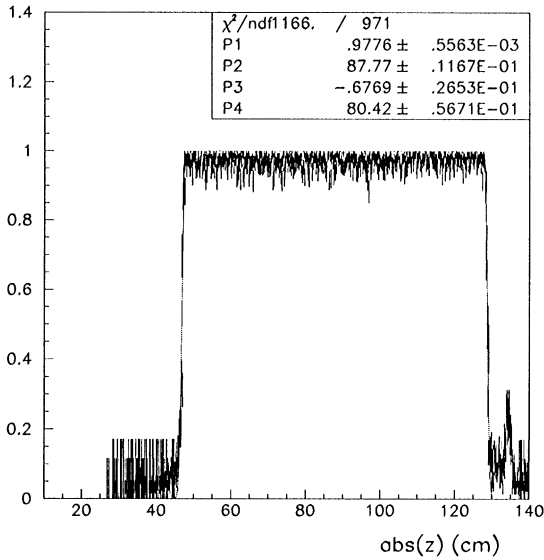
Fig. 11. Cosmic ray efficiency for individual QCAL towers.

χ^2/ndf	1166. / 971
P1	.9776 ± .5563E−03
P2	87.77 ± .1167E−01
P3	−.6769 ± .2653E−01
P4	80.42 ± .5671E−01

Fig. 12. Cosmic ray efficiency as a function of the impact longitudinal coordinate z. At abs$(z) \simeq 135$ cm the small peak corresponds to the photomultiplier position and is probably due to Cherenkov light in the photomultiplier glass.

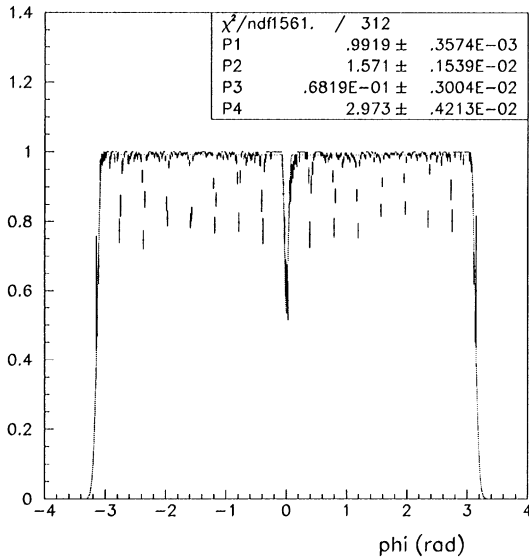| χ^2/ndf	1561. / 312
P1	.9919 ± .3574E−03
P2	1.571 ± .1539E−02
P3	.6819E−01 ± .3004E−02
P4	2.973 ± .4213E−02

Fig. 13. Cosmic ray efficiency as a function of the radial angle ϕ. The loss of efficiency at the module separation ribs is evident, especially at $\phi = 0°$ and $180°$.

evident, in particular at $\phi = 0°$ and $180°$ where the junction of the two support half shells has a thickness of 16 mm of aluminum.

Events from e^+e^- annihilations were used to measure the photon detection efficiency. Two types of events were considered: $K_L \rightarrow \pi^0 \pi^0 \pi^0$ and $K_L \rightarrow \pi^0 \pi^+ \pi^-$. The energy of the photons from the decay of the π^0 is between 20 and 180 MeV. From this sample of events, we selected the ones with one photon missing the EMC barrel or endcap. Then, reconstructing the direction of this photon from the K_L kinematics, we looked for the events where the missing photon was pointing to the QCAL. For these events, we then verified whether there was a hit in the QCAL with the correct time value. As a result, one gets a measured efficiency $\varepsilon_{\mathrm{meas}}$ which is the product of two factors, the intrinsic QCAL efficiency ε times a geometrical contribution $\varepsilon_{\mathrm{res}}$ resulting from the finite resolution in reconstructing the missing photon direction. The latter takes into account the inclusion of events where the photon did not actually hit the QCAL. The result was $\varepsilon_{\mathrm{meas}} = \varepsilon_{\mathrm{res}} \times \varepsilon = (63 \pm 3)\%$ and $(70 \pm 5)\%$ for the $\pi^0 \pi^0 \pi^0$ and $\pi^+ \pi^- \pi^0$ events, respectively. The unknown $\varepsilon_{\mathrm{res}}$ term can be evaluated via Monte Carlo, applying the same procedure to Monte Carlo generated K_L decays. If one can assume that $\varepsilon_{\mathrm{res}} = \varepsilon_{\mathrm{res}}^{\mathrm{MC}}$, one gets $\varepsilon_{\mathrm{res}} = 68\%$ and 76.3% for the charged and neutral events, respectively and the final result $\varepsilon = (92 \pm 4)\%$ for both classes of events.

In order to estimate the accuracy in the photon impact point determination described above, we proceed as follow. We remove one photon from the fully reconstructed (by EMC calorimeter) $K_L \rightarrow \pi^0 \pi^0 \pi^0$ and $K_L \rightarrow \pi^+ \pi^- \pi^0$ events and then subject them to the same analysis as the missing photon events (comparing the inferred photon coordinates with the measured ones). The result was that the photon impact point is reconstructed with an error of $\simeq 15$ cm for the charged events and $\simeq 40$ cm for the neutral ones. The different resolution values are in agreement with the different values of the $\varepsilon_{\mathrm{res}}$ predicted by the Monte Carlo for the two classes of events.

A direct measurement of the photon detection efficiency has been performed using the radiative $e^+e^- \rightarrow \pi^+ \pi^- \gamma$ events (Fig. 14), where the kinematics of the γ is well measured from the charged tracks [6]. These radiative photons come directly from the interaction point and then cross the
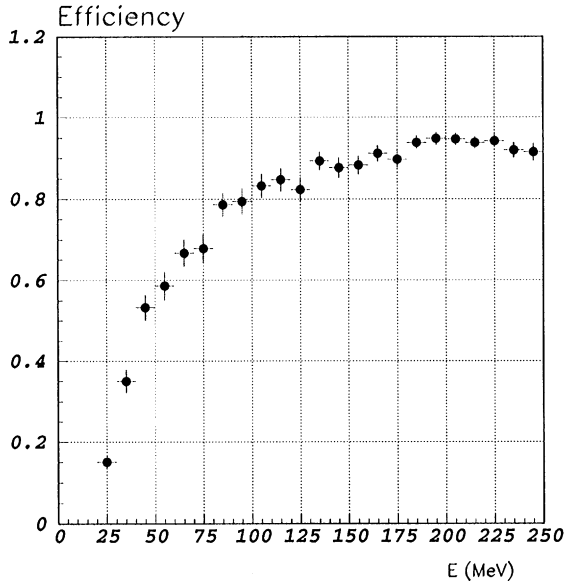
Efficiency

Fig. 14. Photon detection efficiency as a function of the photon energy for the radiative $e^+e^- \to \pi^+\pi^-\gamma$ events.
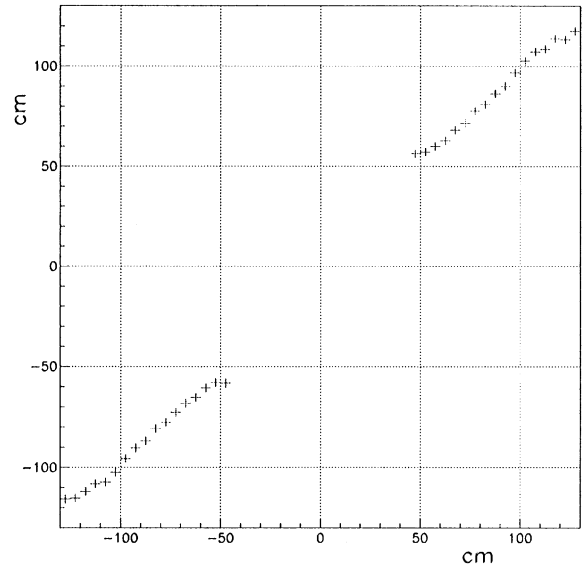

Fig. 15. z coordinate measured by QCAL versus the z calculated with the drift chamber track for cosmic ray events. Each point is the average value of several measurements.

QCAL calorimeter almost along the scintillator and lead layers. For this reason, the photon efficiency is lower with respect to the $K_L \to \pi^0\pi^0\pi^0$ events, where the photons have a higher light yield in QCAL because of the more favorable incident angle.

5.2. Time resolution

The time resolution σ_t can be measured by looking at the resolution along the longitudinal coordinate z, since $\sigma_t = \sigma_z/v$, v being the light speed inside the fiber. If t_1 and t_2 are the signal arrival times at the two optically joined photo-multipliers, we have $z = L - v(t_2 - t_1)/2$ and $t = (t_2 + t_1)/2 - L/v$. Drift chamber information is used to get the precise ($\sigma_z \simeq 3$ mm) position (z_{DC}) of cosmic rays impinging on the QCAL. By comparing this position with the one measured by the QCAL (Fig. 15), we can first determine the best values for the light speed v inside the fibers and the half fiber length L. Fitting the equation $z = L - v(t_2 - t_1)/2$, we found a light speed $v = (18.1 \pm 0.3)$ cm/ns and $L = (98.9 \pm 0.1)$ cm. From Fig. 16, showing the difference $z - z_{DC}$ for one
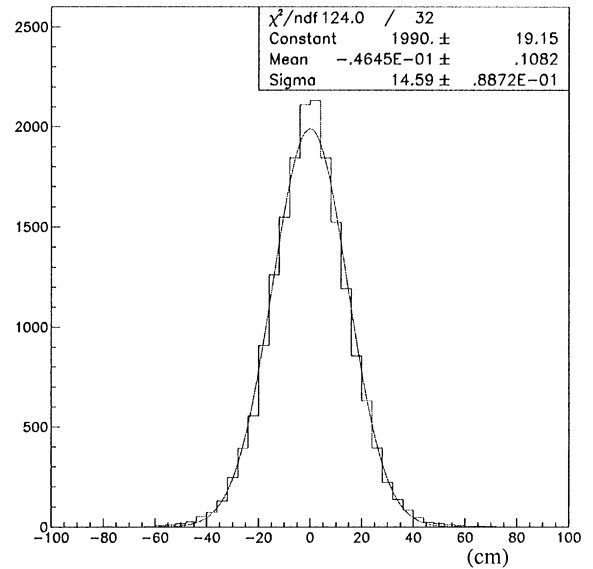

Fig. 16. $z - z_{DC}$ distribution for QCAL A. Since the drift chamber extrapolation has a resolution of about 3 mm, the width of the curve is effectively the QCAL z resolution.

QCAL, we get a value for the resolution $\sigma_z = (16.0 \pm 0.3)$ cm with a resulting time resolution $\sigma_t = (0.88 \pm 0.2)$ ns. Taking into account that a cosmic ray is equivalent to a 75 MeV photon in
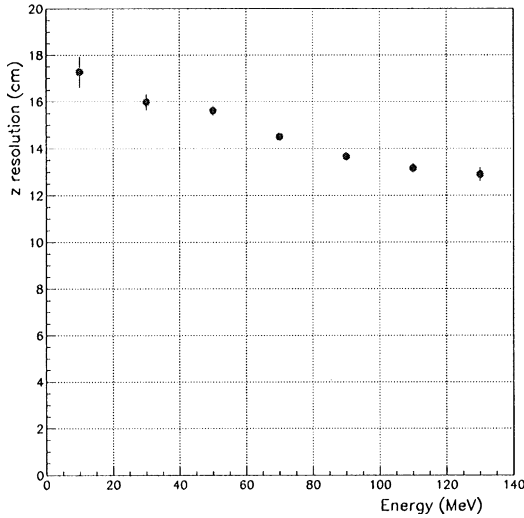
Fig. 17. Resolution of the longitudinal coordinate z as a function of the measured energy.

Fig. 18. $t_{QCAL} - t_{EMC}$ distribution, corrected for the time of flight of the cosmic ray between the EMC and the QCAL and the global EMC t_0, for one QCAL tower. The tower is well calibrated when the distribution is centered at zero.

terms of energy deposit, and that the calorimeter sampling ratio is constant in our energy range, we get $\sigma_t = 240 \text{ ps}/\sqrt{E \text{ (GeV)}}$. This value is in good agreement with the resolution measured in the preliminary test, after accounting for the signal reduction by the magnetic field. Fig. 17 shows the spatial resolution of the longitudinal coordinate z as a function of the MIP measured energy.

5.3. Time and energy calibration

Time and energy calibration were both performed with cosmic rays. Time calibration consisted of putting each QCAL tower in time with the KLOE EMC, which was calibrated separately. The DC information was used to determine the cosmic ray path between the EMC and the QCAL. The cosmic ray tracks were required to cross two elements of both the EMC and the QCAL. Fig. 18 shows the time difference $t_{QCAL} - t_{EMC}$, corrected for the computed cosmic ray TOF, for one QCAL tower. Two hours of normal collision data taking allowed us to acquire enough events to perform a time calibration with a resolution better than 100 ps.

From the preliminary simulation studies, the photon energy resolution was expected always to be larger than 40% but, as pointed out before, the
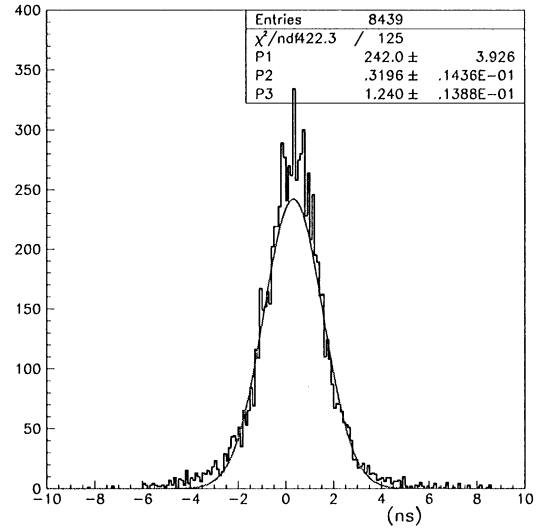
main purpose of the QCAL makes energy resolution relatively less important than efficiency and time resolution. Consequently the energy calibration is not critical. In order to find the right photomultiplier working point, several cosmic ray runs were taken while varying the high voltage from 1700 to 2300 V. In doing the cosmic ray selection, the incident angle of the cosmic ray track was required to be smaller than 30°. Furthermore, the signal was corrected for the effective path inside the tower. An offline adjustment was then performed to force the MIP peak value to be $\simeq 60$ MeV for all the towers (Fig. 20), as predicted by the Monte Carlo simulation. Fig. 19 shows the typical Landau shape of the distribution, with a peak value at 60 MeV and an average energy of 75 MeV.

6. Conclusions

The QCAL calorimeters of the KLOE experiment have been built and are fully operational in the experiment data taking. Average detection efficiencies of 98% and 92% have been measured
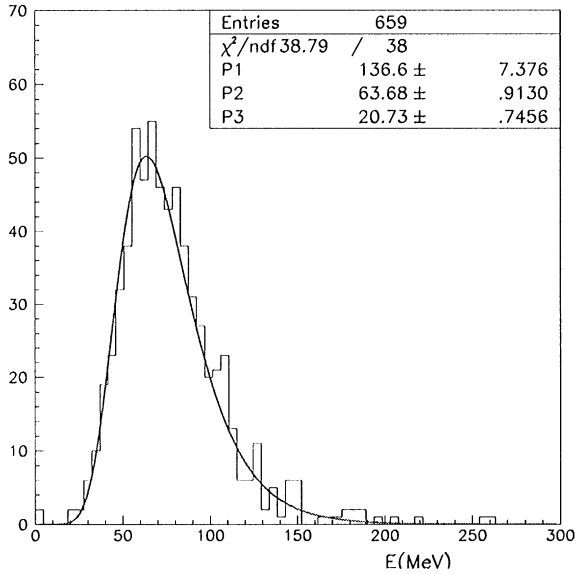
Fig. 19. Energy deposit inside the calorimeter for selected cosmic rays.
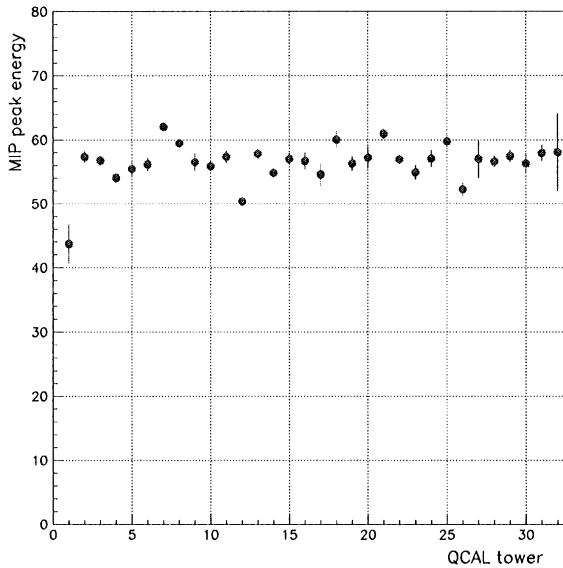

Fig. 20. Cosmic ray energy deposit (MeV) versus tower number. The plotted values refer to the peak of the Landau distribution fit.

for cosmic rays and for photons of $K_L \to \pi^0\pi^0\pi^0$ events, respectively. The measured time resolution is $\sigma_t = 240/\sqrt{E \text{ (GeV)}}$ ps. The performance of the QCAL tile calorimeters shows good agreement with the design parameters and preliminary tests.

References

[1] The KLOE Collaboration, The KLOE detector, technical proposal, LNF-93/002, 1993.
[2] G. Vignola, in: J. Sanford (Ed.), Proceedings of the XXVI International Conference on HEP, AIP, 1992, p. 1941.
[3] E. Santovetti, La reiezione dei fondi sul canale $K_L \to \pi^0\pi^0$ ed il calorimetro sui quadrupoli interni nell'esperimento KLOE, Ph.D. Thesis, Università di Roma Tor Vergata, 1998.
[4] Hamamatsu Photonics K.K., Photomultipliers Tubes and Assemblies, 1995.
[5] The KLOE Collaboration, The KLOE data acquisition system (addendum to the KLOE technical proposal), LNF-94/014, 1995.
[6] G. Cataldi, et al., Measurement of the hadronic cross section $\sigma(e^+e^- \to \pi^+\pi^-)$ from initial state radiative events ($\pi^+\pi^-\gamma$) with the KLOE detector, KLOE Memo 195, 1999.
[7] A. Antonelli, et al., GEANFI Handbook vers. 1.3.3, KLOE Internal Note 52-3/93, 1993.
[8] M. Adinolfi, et al., Readout optimization for the KLOE QCAL tile calorimeters, Proceedings of the Seventh Pisa Meeting on Advanced Detectors, La Biodola, Nucl. Instr. and Meth. A 409 (1998) 613.